Thermodynamics of the Stockmayer fluid in an applied field

To appear in *Molecular Physics*
Vol. 00, No. 00, May 2015, 1–20

ARTICLE

Thermodynamics of the Stockmayer fluid in an applied field

Ekaterina A. Elfimova[a], Alexey O. Ivanov[a], Julien O. Sindt[b] and Philip J. Camp[b*]

[a] *Institute of Mathematics and Computer Sciences, Ural Federal University, 51 Lenin Avenue, Ekaterinburg 620000, Russia*
[b] *School of Chemistry, University of Edinburgh, David Brewster Road, Edinburgh, EH9 3FJ, Scotland*

(*June 17, 2015*)

The thermodynamic properties of the Stockmayer fluid in an applied field are studied using theory and computer simulation. Theoretical expressions for the second and third virial coefficients are obtained in terms of the dipolar coupling constant (λ, measuring the strength of dipolar interactions as compared to thermal energy) and dipole-field interaction energy (α, being proportional to the applied field strength). These expressions are tested against numerical results obtained by Mayer sampling calculations. The expression for the second virial coefficient contains terms up to λ^4, and is found to be accurate over realistic ranges of dipole moment and temperature, and over the entire range of the applied field strength (from zero to infinity). The corresponding expression for the third virial coefficient is truncated at λ^3, and is not very accurate: higher order terms are very difficult to calculate. The virial coefficients are incorporated in to a thermodynamic theory based on a logarithmic representation of the Helmholtz free energy. This theory is designed to retain the input virial coefficients, and account for some higher order terms in the sense of a resummation. The compressibility factor is obtained from the theory and compared to results from molecular dynamics simulations with a typical value $\lambda = 1$. Despite the mathematical approximations of the virial coefficients, the theory captures the effects of the applied field very well. Finally, the vapour-liquid critical parameters are determined from theory, and compared to published simulation results; the agreement between theory and simulation is good.

Keywords: Stockmayer fluid; applied field; theory; simulation

1. Introduction

One of the most widely studied, simple models of polar materials is based on the Stockmayer interaction potential. In this model, the constituent particles are Lennard-Jones (LJ) particles carrying a central point dipole moment $\boldsymbol{\mu}$. Thus, the interaction potential between any pair of particles i and j is given by a sum of LJ and dipolar (d) contributions as follows.

$$u_{ij} = u_{ij}^{\mathrm{LJ}} + u_{ij}^{\mathrm{d}} \tag{1}$$

$$u_{ij}^{\mathrm{LJ}} = 4\epsilon \left[\left(\frac{\sigma}{r_{ij}} \right)^{12} - \left(\frac{\sigma}{r_{ij}} \right)^{6} \right] \tag{2}$$

$$u_{ij}^{\mathrm{d}} = \frac{(\boldsymbol{\mu}_i \cdot \boldsymbol{\mu}_j)}{r_{ij}^3} - \frac{3(\boldsymbol{\mu}_i \cdot \boldsymbol{r}_{ij})(\boldsymbol{\mu}_j \cdot \boldsymbol{r}_{ij})}{r_{ij}^5} \tag{3}$$

*Corresponding author. E-mail: philip.camp@ed.ac.uk

ISSN: 00268976 print/ISSN 13623028 online

DOI: 10.1080/0026897YYxxxxxxxx
http://www.informaworld.com

Here ϵ is the LJ interaction well depth, σ is the particle diameter, and $r_{ij} = |\boldsymbol{r}_{ij}|$ is the length of the centre-centre vector $\boldsymbol{r}_{ij}$. Historically, this model was introduced to describe the virial coefficients and thermodynamic properties of 'simple' polar fluids such as ammonia or water, in which the dispersion and dipole-dipole interactions affect the bulk properties to comparable extents [1–4].

Such models are useful for describing the properties of polar particles in general [5], including *colloidal* magnetised particles such as those used to make ferrofluids [6]. In these materials, the particles are roughly spherical, nanometre-sized, homogeneously magnetised grains, sterically stabilised and suspended in an inert carrier liquid. Approximating the particles to be perfect spheres, the dipolar interaction is precisely that given in Equation (3). In some ferrofluid models, the short-range interactions are given by a simple hard-sphere repulsion, giving the dipolar hard sphere (DHS) model. In general, though, unless the carrier liquid is refractive-index matched, some sort of short-range attraction is expected between the particles, and so the total interaction given by Equation (1) is more appropriate. Of course, the functional form of the total van der Waals interactions between colloidal particles is different from that given in Equation (2). Nonetheless such 'atomic' models can provide excellent descriptions of the properties of bulk ferrofluids. For example, the magnetisation curves and initial susceptibilities of real ferrofluids can be matched almost identically by those from theory and simulations of such simple models [7, 8], including the effects of particle dispersity [9, 10].

The most important control parameters of the Stockmayer model are the thermal energy ($k_{\mathrm{B}}T$), the LJ energy (ϵ), and the characteristic dipolar energy (μ^2/σ^3). Hence, three important dimensionless quantities are the reduced temperature T^*, the reduced dipole moment μ^*, and the dipolar coupling constant λ defined as follows.

$$T^* = \frac{k_{\mathrm{B}}T}{\epsilon} \tag{4}$$

$$\mu^* = \frac{\mu}{\sqrt{\epsilon\sigma^3}} \tag{5}$$

$$\lambda = \frac{\mu^2}{k_{\mathrm{B}}T\sigma^3} = \frac{(\mu^*)^2}{T^*} \tag{6}$$

In computer simulations of the Stockmayer model, it was shown that with large dipole moments – such that the dipolar interactions dominate – chaining of the particles in a nose-to-tail parallel conformation ($\rightarrow\rightarrow$) suppresses a conventional vapour-to-liquid phase transition [11–13], or at least leads to deviations from 'normal' corresponding-states relationships between the critical parameters. The dipolar limit ($\mu^* \rightarrow \infty$) has been a matter of debate for over four decades. On the basis of a large number of simulation studies of Stockmayer, DHS, and related models [14–37], the existence of a purely dipole-driven vapour-liquid transition now seems unlikely, with several studies showing that a small contribution from other interactions (arising from, e.g., higher multipolar interactions, dispersion interactions, non-spherical particles, non-polar additives, etc.) is required for condensation to occur [28, 32, 34, 37].

Another important variable is, of course, an applied field $\boldsymbol{H}$, which gives rise to an additional energetic contribution of

$$\psi_i = -\boldsymbol{\mu}_i \cdot \boldsymbol{H} \tag{7}$$

for particle i. The dimensionless field H^*, and a field-dipole interaction energy α

can be defined by

$$H^* = H\sqrt{\frac{\sigma^3}{\epsilon}} \tag{8}$$

$$\alpha = \frac{\mu H}{k_{\rm B}T} = \frac{\mu^* H^*}{T^*} \tag{9}$$

where $H = |\boldsymbol{H}|$. The dependence of the vapour-liquid critical parameters of the Stockmayer fluid in an applied field has been examined using computer simulations by Stevens and Grest [20], Boda *et al.* [22], and Kristóf *et al.* [25]. In general, as H^* is increased, the critical temperature increases by up to about 40%, while the critical concentration remains roughly constant.

From the theoretical standpoint, there are many approaches to the general problem of how to describe the thermodynamic and structural properties of dipolar fluids in applied fields, including density functional theory [38, 39], integral equations [39–41], and thermodynamic perturbation theory [42]. The authors have developed virial expansions, and improvements thereon, that provide explicit expressions for thermodynamic and structural functions [43, 44] which compare very well with computer-simulation data. A simple resummation of the virial expansion, based on a logarithmic form for the free energy, gives a convenient and accurate expression for the equation of state [44, 45]. Along the way, it has been emphasised that the basic definitions of the virial coefficients contain additional terms related to the field; this was anticipated in earlier work by additional terms related to intramolecular degrees of freedom [46, 47]. Explicit expressions for the virial coefficients have been developed, and compared with the results from Mayer-sampling calculations [48]. Up until now, the virial and related expansions have only been tested on DHS models. The aim of the current work is to extend this formalism to systems with additional, non-dipolar interactions. A logical starting point is therefore to study the Stockmayer fluid in an applied field. To this end, theory and simulation are combined to obtain virial coefficients and thermodynamic properties as functions of T^*, λ, and α.

This article is organised as follows. Section 2 contains explicit expressions for the virial coefficients, and a summary of various virial-expansion theories. Computational details are given in Section 3. The results are presented in Section 4, beginning with a systematic survey of virial coefficients, and then moving on to comparisons between the equation of state and vapour-liquid critical parameters from theory and simulation. The conclusions are given in Section 5.

2. Theory

The theory of N Stockmayer particles in a volume V, and in an applied field H, begins with the regular virial expansion (VE) of the compressibility factor Z given by

$$Z = \frac{\beta P}{\rho} = 1 + \sum_{n=1}^{\infty} B_{n+1}\rho^n \tag{10}$$

where $\beta = 1/k_{\rm B}T$, P is the pressure, $\rho = N/V$ is the concentration, and B_n are virial coefficients. The virial coefficients become ever more difficult to calculate as n increases. The rate of convergence of the virial series can be very slow and/or the signs of the virial coefficients can alternate, frustrating attempts to improve

the accuracy of the expansion simply by adding extra terms. One approach to this problem is to introduce a perturbed virial expansion (PVE) of the form

$$Z = Z^{\text{ref}} + \sum_{n=1}^{\infty} \Delta B_{n+1} \rho^n \tag{11}$$

where Z^{ref} is the compressibility factor of a reference system, and $\Delta B_n = B_n - B_n^{\text{ref}}$ is the difference between the virial coefficients of the system of interest and the reference system [49–53]. The idea behind this approach is that, if the properties of a reference system are well known (e.g., hard-sphere fluid, LJ fluid), and the system of interest is not too different from the reference system, then the expansion in ρ should make a relatively small contribution, and hopefully converge rapidly.

A related approach is to recast a perturbed virial expansion of the Helmholtz free energy F in to a logarithmic form [44, 45]. The Helmholtz free energy for a system of particles in an applied field can be written

$$\frac{\beta F}{N} = \frac{\beta F^{\text{ref}}}{N} - \ln \Psi + \sum_{n=1}^{\infty} \frac{1}{n} \Delta B_{n+1} \rho^n \tag{12}$$

where F^{ref} is the Helmholtz free energy of a reference system, and

$$\Psi = \int \mathrm{d}\boldsymbol{\Omega} e^{-\beta\psi} = \frac{4\pi \sinh \alpha}{\alpha} \tag{13}$$

is the internal partition function of a particle arising from integrating over its angular coordinates $\boldsymbol{\Omega}$, with ψ given by Equation (7). The so-called logarithmic free energy (LFE) theory is obtained by rewriting Equation (12) in the form

$$\frac{\beta F}{N} = \frac{\beta F^{\text{ref}}}{N} - \ln \Psi - \ln \left(1 + \sum_{n=1}^{\infty} \frac{1}{n} I_{n+1} \rho^n \right). \tag{14}$$

Matching terms between Equation (12) and a Maclaurin expansion of (14) gives for the first two coefficients

$$I_2 = -\Delta B_2 \tag{15}$$

$$I_3 = -\Delta B_3 + \Delta B_2^2. \tag{16}$$

The compressibility factor can then be obtained easily from the Helmholtz free energy as follows.

$$Z = \rho \frac{\partial}{\partial \rho} \left(\frac{\beta F}{N} \right) = Z^{\text{ref}} - \frac{I_2 \rho + I_3 \rho^2}{1 + I_2 \rho + \frac{1}{2} I_3 \rho^2} \tag{17}$$

The prefactor of the logarithmic term in Equation (14) can be $+1$ or -1, but in the presence of attractive interactions, the net contribution is expected to be negative. Choosing a factor of -1 means that the argument of the logarithm should remain positive, and therefore it should not accidentally turn negative at high values of ρ. The LFE theory has been tested against simulation results for DHSs with and without an applied field [44, 45]. The LFE theory outperforms the PVE theory for this system. The reason is that the logarithmic form of the Helmholtz free

energy includes terms of higher order in ρ than the level of truncation inside the logarithm. Although these higher order terms are given only approximately, it appears that knowledge of the second and third virial coefficients is sufficient to get good agreement with simulation data up to quite high concentrations (up to about 40% volume fraction) and (for ferrofluids) low temperatures $\lambda \leq 2$.

In this work, the reference system is taken to be the LJ fluid, which is itself described in terms of the hard-sphere (HS) fluid plus a perturbation at the PVE level [Equation (11)]. Nezbeda and co-workers have found this type of approach to provide a very accurate description of the LJ fluid [51, 52], and this is confirmed in Sections 4.2 and 4.3 where it is compared with simulation results. The effective hard-sphere diameter d is determined using the familiar Barker-Henderson formula [54, 55] with the repulsive term (u_{ij}^{r}) in the following partitioning of the LJ potential [42].

$$u_{ij}^{\mathrm{r}} = \begin{cases} u_{ij}^{\mathrm{LJ}} & r_{ij} < \sigma \\ 0 & r_{ij} \geq \sigma \end{cases} \tag{18}$$

$$u_{ij}^{\mathrm{a}} = \begin{cases} 0 & r_{ij} < \sigma \\ u_{ij}^{\mathrm{LJ}} & r_{ij} \geq \sigma \end{cases} \tag{19}$$

The HS compressibility factor (Z^{HS}) is given accurately by the Carnahan-Starling result [55, 56]. The final expression for the compressibility factor of the reference LJ fluid is then

$$Z^{\mathrm{ref}} = Z^{\mathrm{HS}} + (B_2^{\mathrm{LJ}} - B_2^{\mathrm{HS}})\rho + (B_3^{\mathrm{LJ}} - B_3^{\mathrm{HS}})\rho^2 \tag{20}$$

with the HS virial coefficients $B_2^{\mathrm{HS}} = 2\pi d^3/3$ and $B_3^{\mathrm{HS}} = 5\pi^2 d^6/18$.

2.1. *Virial coefficients*

The correct expressions for the second and third virial coefficients of a system in an applied field were derived in Reference 44. The second virial coefficient is given by

$$B_2 = -\frac{1}{2}\int \mathrm{d}\boldsymbol{r}_{12}\langle f_{12}\rangle \tag{21}$$

where

$$f_{ij} = \exp\left(-\beta u_{ij}\right) - 1 \tag{22}$$

is the Mayer f-function, and the angular brackets denote a Boltzmann-weighted, orientational average for each particle. The explicit expression in this case is

$$\langle f_{12}\rangle = \frac{1}{\Psi^2}\int \mathrm{d}\boldsymbol{\Omega}_1 \int \mathrm{d}\boldsymbol{\Omega}_2 f_{12} e^{-\beta(\psi_1+\psi_2)}. \tag{23}$$

The third virial coefficient is expressed conveniently as a sum of two terms:

$$B_3 = B_{3a} + B_{3b}. \tag{24}$$

B_{3a} is an orientational average of the familiar, zero-field expression, while B_{3b} is more complex.

$$B_{3a} = -\frac{1}{3}\int \mathrm{d}\boldsymbol{r}_{12}\int \mathrm{d}\boldsymbol{r}_{13}\langle f_{12}f_{13}f_{23}\rangle \tag{25}$$

$$B_{3b} = \int \mathrm{d}\boldsymbol{r}_{12}\int \mathrm{d}\boldsymbol{r}_{13}[\langle f_{12}\rangle\langle f_{13}\rangle - \langle f_{12}f_{13}\rangle] \tag{26}$$

In the absence of an applied field, or in the presence of an infinitely strong field, $\langle f_{12}\rangle\langle f_{13}\rangle = \langle f_{12}f_{13}\rangle$, and hence $B_{3b} = 0$. For DHSs in the presence of finite fields, B_{3b} was found to give a small but significant negative contribution to B_3 on the order of 10% [44]. It is emphasised that these 'fluctuation' corrections to the virial coefficients were first identified by Caracciolo *et al.* as arising from intramolecular degrees of freedom [46, 47].

The task now is to develop explicit expressions for B_2 and B_3 in terms of T^*, λ, and α, these representing the strengths of the LJ, dipole-dipole, and dipole-field interactions, respectively. To begin, the repulsive interaction potential u_{ij}^{r} is replaced by the hard-sphere (HS) potential.

$$u_{ij}^{\mathrm{HS}} = \begin{cases} \infty & r_{ij} < d \\ 0 & r_{ij} \geq d \end{cases} \tag{27}$$

With this substitution, the Mayer f-function for the LJ potential can now be approximated by

$$f_{ij}^{\mathrm{LJ}} \simeq \exp\left(-\beta u_{ij}^{\mathrm{HS}} - \beta u_{ij}^{\mathrm{a}}\right) - 1 = f_{ij}^{\mathrm{HS}} + (f_{ij}^{\mathrm{HS}}+1) f_{ij}^{\mathrm{a}} = f_{ij}^{\mathrm{HS}} + (f_{ij}^{\mathrm{HS}}+1)\sum_{k=1}^{\infty}\frac{(-\beta u_{ij}^{\mathrm{a}})^k}{k!}. \tag{28}$$

To obtain the Mayer f-function for the Stockmayer fluid, the dipolar interaction can be added in a similar way as follows.

$$f_{ij} = \exp\left(-\beta u_{ij}^{\mathrm{LJ}} - \beta u_{ij}^{\mathrm{d}}\right) - 1 = f_{ij}^{\mathrm{LJ}} + (f_{ij}^{\mathrm{LJ}}+1) f_{ij}^{\mathrm{d}} = f_{ij}^{\mathrm{LJ}} + (f_{ij}^{\mathrm{LJ}}+1)\sum_{l=1}^{\infty}\frac{(-\beta u_{ij}^{\mathrm{d}})^l}{l!} \tag{29}$$

Inserting Equation (28) for $(f_{ij}^{\mathrm{LJ}}+1)$ in Equation (29) gives an expansion of f_{ij} in terms of $\beta u_{ij}^{\mathrm{a}}$ and $\beta u_{ij}^{\mathrm{d}}$.

$$f_{ij} = f_{ij}^{\mathrm{LJ}} + (f_{ij}^{\mathrm{HS}}+1)\sum_{k=0}^{\infty}\sum_{l=1}^{\infty}\frac{(-\beta u_{ij}^{\mathrm{a}})^k(-\beta u_{ij}^{\mathrm{d}})^l}{k!l!} \tag{30}$$

The calculations of B_2, B_{3a}, and B_{3b} from Equations (21), (25), and (26), respectively, bring in additional dependences on α from the orientational averages. The calculations are laborious: some of the required integrals have been determined in earlier work [44], and new results are given in the Appendices.

2.1.1. B_2

The non-polar contribution to B_2 can be calculated numerically.

$$B_2^{\mathrm{LJ}} = -\frac{1}{2}\int \mathrm{d}\boldsymbol{r}_{12} f_{12}^{\mathrm{LJ}} \tag{31}$$

The dipolar contributions arising from the sum in Equation (29) are brought in by calculating terms up to $k+l=4$ in Equation (30). The individual terms are given in Appendix A, but the final result is

$$\begin{aligned}\frac{B_2}{b} &= \frac{B_2^{\mathrm{LJ}}}{b} \\ &- \lambda L^2(\alpha) \\ &- \frac{\lambda^2[5+L_3^2(\alpha)]}{15}\left[\frac{\sigma^3}{d^3}+\frac{8}{15T^*}+\frac{64}{315(T^*)^2}\right] \\ &- \frac{\lambda^3}{105}\left[\frac{2L(\alpha)L_3(\alpha)}{\alpha}-\frac{5L_3^2(\alpha)}{\alpha^2}+4L^2(\alpha)\right]\left(\frac{\sigma^6}{d^6}+\frac{2}{3T^*}\right) \\ &- \frac{\lambda^4}{420}\frac{\sigma^9}{d^9}\left[\frac{116L^2(\alpha)}{\alpha^2}-\frac{44L(\alpha)}{\alpha}-\left(\frac{395}{\alpha^3}-\frac{28}{\alpha}\right)L(\alpha)L_3(\alpha)\right. \\ &\left.- \left(\frac{105}{\alpha^2}-\frac{140}{\alpha^4}\right)L_3^2(\alpha)+\frac{113L_3(\alpha)}{\alpha^2}+8\right] \end{aligned} \tag{32}$$

where $b=2\pi\sigma^3/3$, $L(\alpha)=[\coth(\alpha)-\alpha^{-1}]$ is the Langevin function, and $L_n(\alpha)=1-nL(\alpha)/\alpha$.

2.1.2. B_3

The non-polar contribution to B_3 can be calculated numerically, using the LJ potential directly.

$$B_2^{\mathrm{LJ}} = -\frac{1}{3}\int \mathrm{d}\boldsymbol{r}_{12}\int \mathrm{d}\boldsymbol{r}_{13} f_{12}^{\mathrm{LJ}} f_{13}^{\mathrm{LJ}} f_{23}^{\mathrm{LJ}} \tag{33}$$

The evaluation of the dipolar contributions to B_3 is considerably more complex, and so the expansions of Equations (25) and (26) are truncated at manageable levels. B_{3a} and B_{3b} have been determined up to the terms involving $(-\beta u_{ij}^{\mathrm{d}})$, $(-\beta u_{ij}^{\mathrm{d}})(-\beta u_{ij}^{\mathrm{a}})$, $(-\beta u_{ij}^{\mathrm{d}})^2$, and $(-\beta u_{ij}^{\mathrm{d}})^3$. Some further comments are made in Appendix B, but the final result for B_3 is

$$\begin{aligned}\frac{B_3}{b^2} &= \frac{B_3^{\mathrm{LJ}}}{b^2} \\ &- \frac{\lambda^2}{8}\left\{\left(2\ln 2+\frac{1}{3}\right)\left[1+\frac{L_3^2(\alpha)}{5}\right]-2L^2(\alpha)\left[16L^2(\alpha)+\frac{29L(\alpha)}{\alpha}-10\right]\right\} \\ &- \frac{\lambda^3}{8}\left\{(292+12\ln 2)\frac{L^3(\alpha)}{5\alpha}+(288\ln 2-174)\frac{L^3(\alpha)}{\alpha^3}-\frac{64L^2(\alpha)L_3^2(\alpha)}{15}\right. \\ &+ \left(\frac{112}{5}+\frac{48\ln 2}{35}\right)L^2(\alpha)L_3(\alpha)+(192\ln 2-146)\frac{L^2(\alpha)L_3(\alpha)}{\alpha^2} \\ &+ (48-96\ln 2)\frac{L^2(\alpha)}{\alpha^2}-\frac{3686L^2(\alpha)}{175}+\frac{20L(\alpha)L_2(\alpha)L_3(\alpha)}{\alpha} \\ &+ \left(\frac{1884\ln 2}{7}-188\right)\frac{L(\alpha)L_3^2(\alpha)}{\alpha}+\frac{71L(\alpha)L_3(\alpha)}{525\alpha}+(48-96\ln 2)L_2^2(\alpha)L_3(\alpha) \\ &\left.+ (232-384\ln 2)\frac{L_2(\alpha)L_3^2(\alpha)}{5}+\left(\frac{864\ln 2}{5}-\frac{3384}{35}\right)L_3^3(\alpha)-\frac{71L_3^2(\alpha)}{210\alpha^2}\right\} \end{aligned} \tag{34}$$

With B_2 and B_3 in hand, it is straightforward to calculate the expansion coefficients in the LFE expressions – Equations (14) and (17) – using the definitions given by Equations (15) and (16). Specifying the LJ fluid as the reference system, $\Delta B_2 = B_2 - B_2^{\rm LJ}$ and $\Delta B_3 = B_3 - B_3^{\rm LJ}$. The compressibility factor of the Stockmayer fluid is then given by Equation (17) with $Z^{\rm ref}$ given by Equation (20). Once again, it is emphasised that the reference LJ system is described at the PVE level, starting from the HS fluid. The dipolar corrections to the LJ fluid are then handled at the LFE level. Variants of the theory could include the LJ and dipolar corrections handled at either the PVE or LFE levels, but the choice made here was found to provide the best agreement with simulation, as will be demonstrated in Sections 4.2 and 4.3.

3. Computer simulations

3.1. *Mayer sampling*

The second virial coefficient was determined using Mayer sampling [48]. In this method, two-particle configurations are sampled according to a weight w, chosen to reflect the configurations that make the most significant contributions to the quantity of interest, in this case B_2. The weight was chosen to be $w = |f_{12}e^{-\beta(\psi_1+\psi_2)}|$ [see Equation (23)]. If B_2 is known for a reference system (call it $B_2^{\rm ref}$) then

$$\frac{B_2}{B_2^{\rm ref}} = \frac{\langle f_{12}e^{-\beta(\psi_1+\psi_2)}/w\rangle_w}{\langle f_{12}^{\rm ref}e^{-\beta(\psi_1+\psi_2)}/w\rangle_w} \tag{35}$$

where $\langle\ldots\rangle_w$ denotes an average over the biased distribution of configurations with weight w. The dipolar interaction introduces a complication, however, because the long-range contribution to f_{12}, proportional to $-\beta u_{12}^{\rm d}$, depends on the shape of the sample container due to depolarisation fields. In both theory and simulation, it is most convenient to consider a case where the depolarisation fields vanish, and this corresponds to a cylindrical container of infinite aspect ratio. With this choice, the long-range part can be evaluated straightforwardly. Hence, Mayer sampling is used to evaluate the integral of

$$\Delta f_{12} = f_{12} + (f_{12}^{\rm LJ} + 1)\beta u_{12}^{\rm d} \tag{36}$$

which has no long-range term $\sim \beta u_{12}^{\rm d}$. B_2 is then obtained by adding in the result of integrating the long-range part analytically [44]; note that the long-range part does not depend on the form of the short-range interaction.

$$B_2 = -\frac{1}{2}\int {\rm d}\boldsymbol{r}_{12}\langle\Delta f_{12}\rangle - b\lambda L^2(\alpha) \tag{37}$$

As discussed in detail in Reference 44, B_{3a} (25) can be calculated directly using Mayer sampling because there are no terms that depend on sample geometry. Unfortunately, B_{3b} does contain such contributions: the offending term is the integral of $\langle\beta u_{12}^{\rm d}\Delta f_{13}\rangle$, and further expansion of Δf_{13} in terms of λ shows that there are contributions of all orders; therefore, the coefficient in front of this long-range term cannot be evaluated analytically. The comparison between theory and simulation will be limited here to B_2 and B_{3a}, but in practice B_{3b} is anyway quite small compared to B_{3a}.

For best results, the reference system should be chosen so that there is a reasonable overlap between the configurations that make major contributions to B_n and B_n^{ref}. In this work, the reference system was taken as hard spheres, with a diameter chosen to minimise statistical errors; by trial and error, the optimum hard-sphere diameter was found to be 1.6σ.

3.2. *Molecular dynamics simulations*

Canonical (NVT) molecular dynamics (MD) simulations were carried out using LAMMPS [57, 58]. $N = 512$ Stockmayer particles were simulated in a uniform field with periodic boundary conditions applied. The long-range dipolar interactions were computed using Ewald summations with conducting boundary conditions, which removes depolarisation fields [59]. The equations of motion were integrated using the velocity-Verlet method, with a reduced timestep $\delta t^* = 0.01$. Constant-temperature conditions were achieved using a Langevin thermostat. A typical run consisted of 5×10^5 timesteps for equilibration, followed by a production run of the same length. Averages were calculated from measurements taken at intervals of 100 timesteps.

4. Results

The virial coefficients, equation of state, and vapour-liquid critical parameters are considered in turn.[1]

4.1. *Virial coefficients*

Figure 1 shows the second virial coefficient B_2 in zero applied field ($\alpha = 0$) as a function of reduced temperature T^* and with fixed reduced dipole moments $\mu^* = 0$, $1/\sqrt{2}$, 1, and $\sqrt{2}$. Results are shown from theory and Mayer-sampling calculations. For a given dipole moment, B_2 becomes more negative with decreasing temperature. Similarly, for a given temperature, increasing the dipole moment leads to a decrease in B_2. These trends are simply due to the contributions from the attractive interactions becoming more prominent. With $\mu^* = 0$ the agreement between theory and Mayer sampling is perfect because the LJ contribution is computed directly from Equation (31). This good agreement is maintained with increasing μ^*, with only minor deviations setting in at $\mu^* = \sqrt{2}$ and at temperatures approaching $T^* = 1$.

Figure 2 shows corresponding results for the third virial coefficient B_3 in zero applied field ($\alpha = 0$). Also shown in Figure 2(a) are some numerical results taken from Table II of Reference 4, but these are obscured by the new Mayer-sampling results. B_3 shows a global maximum which increases with increasing μ^*, and shifts to lower temperature. As before, with $\alpha = 0$, the agreement between theory and Mayer sampling is perfect because the LJ contribution is computed directly from Equation (33). With increasing μ^*, the agreement between theory and Mayer sampling worsens, due to truncation of the λ-expansion at third order in Equation (34). Nonetheless, the basic shapes of the functions are correct, and the theoretical and numerical results converge at high temperature, as they should.

[1]Original data from Mayer-sampling and molecular-dynamics simulations are available from http://dx.doi.org/10.7488/ds/249

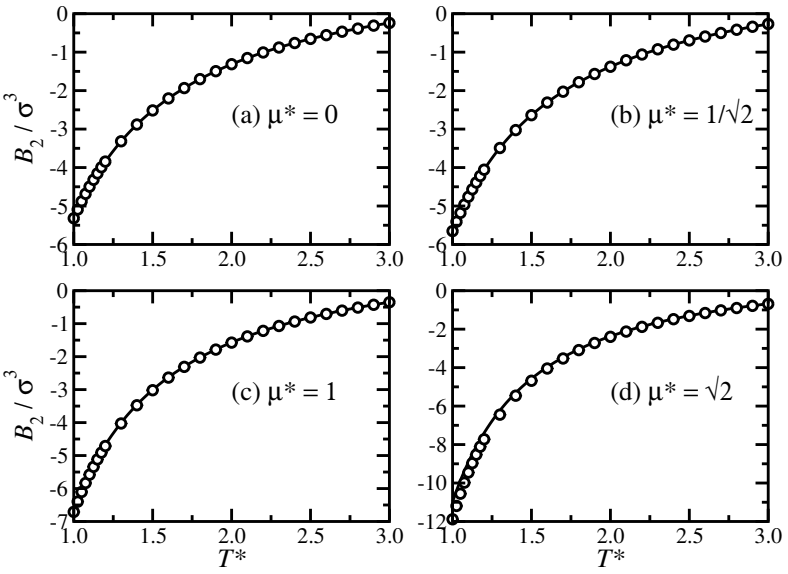

Figure 1. Second virial coefficient B_2 as a function of T^* in zero applied field ($\alpha = 0$): (a) $\mu^* = 0$; (b) $\mu^* = 1/\sqrt{2}$; (c) $\mu^* = 1$; (d) $\mu^* = \sqrt{2}$. The open symbols are from Mayer sampling, and the lines are from theory.

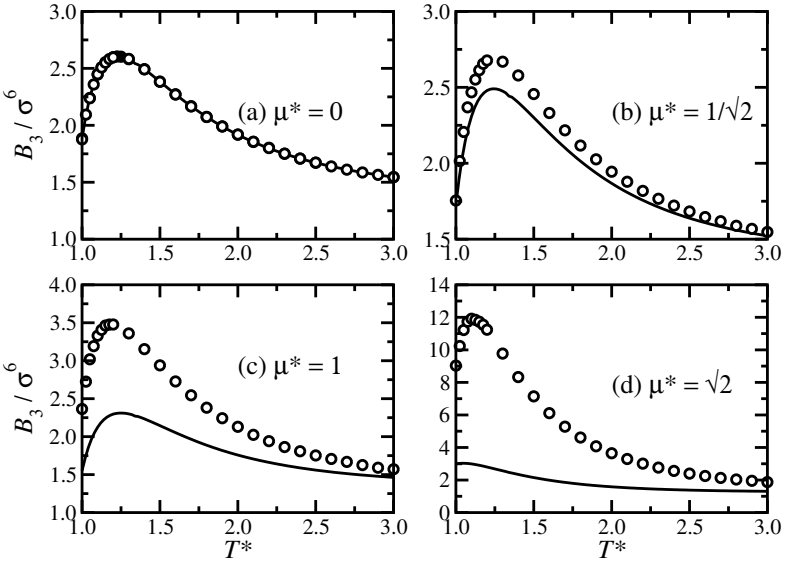

Figure 2. Third virial coefficient B_3 as a function of T^* in zero applied field ($\alpha = 0$): (a) $\mu^* = 0$; (b) $\mu^* = 1/\sqrt{2}$; (c) $\mu^* = 1$; (d) $\mu^* = \sqrt{2}$. The open symbols are from Mayer sampling, and the lines are from theory. In (a) there are also results taken from Table II of Reference 4 (filled symbols) but they are obscured by the new Mayer-sampling results.

It is useful to reconsider the results at fixed λ instead of at fixed μ^*. While the electric dipole moment of a molecule is basically fixed by chemical bonding, there are various ways of altering the magnetic dipole moment of a nanoparticle or other colloidal particle, such as with temperature, chemical composition, particle size, etc. Therefore, when discussing magnetic particles and ferrofluids, it is more usual to characterise the strength of the dipolar interactions by reference to the thermal energy, i.e., by calculating λ. Keeping λ fixed and varying T^* is like changing the strength of the non-magnetic, van der Waals attractions between ferrofluid particles at fixed T, which could be achieved by varying the refractive-index (mis)match between the particles and the suspending liquid.

Figures 3 and 4 show, respectively, the second virial coefficient B_2 and third

virial coefficient B_3 in zero applied field ($\alpha = 0$) as functions of temperature T^* and with fixed $\lambda = 0$, $1/2$, 1, and 2. These choices of λ correspond to $\mu^* = 0$, $1/\sqrt{2}$, 1, and 2, respectively, at a temperature $T^* = 1$. The results for B_2 in Figure 3 show that there is excellent agreement between theory and Mayer sampling up to $\lambda = 1$, while at $\lambda = 2$ there are deviations on the order of 10% at the lowest temperatures. This is encouraging, because the dipolar coupling constants in real ferrofluids are rarely higher than 1. Over this temperature range, the additional van der Waals interactions simply make B_2 more negative because the configurations of particles giving attractive dipolar interactions (i.e., parallel, nose-to-tail configurations) just become even more dominant in the configurational integral (21).

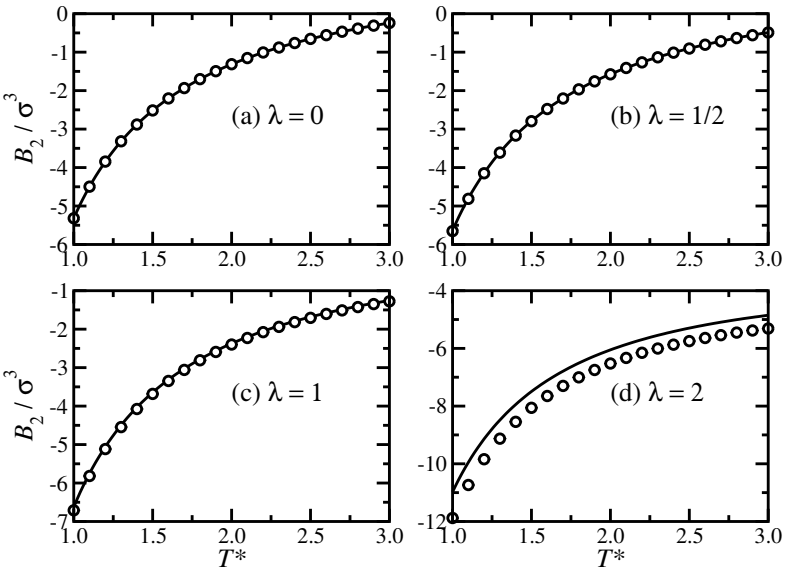

Figure 3. Second virial coefficient B_2 as a function of T^* in zero applied field ($\alpha = 0$): (a) $\lambda = 0$; (b) $\lambda = 1/2$; (c) $\lambda = 1$; (d) $\lambda = 2$. The open symbols are from Mayer sampling, and the lines are from theory.

Figure 4 shows that the theoretical description of B_3 is far less satisfactory. The agreement between theory and Mayer sampling is worse here than in Figure 2 because the dipolar interaction strength is kept constant with respect to the thermal energy. Hence, the deviations do not decrease with increasing temperature. Note that some points from Reference 4 are included in the figure, as a check of the new Mayer-sampling results with $\lambda = 0$.

To complete the discussion of the zero-field case, Figure 5 shows the variations of B_2 and B_3 with λ at various fixed temperatures. The behaviour of B_2 is unremarkable, simply decreasing with increasing λ as the attractive dipolar interactions arising from chain-like configurations increase in significance. Basically, the theory captures this effect quantitatively up until $\lambda \simeq 1$, and then beyond that value significant deviations become apparent. This is a simple consequence of the truncation of the expansion in Equation (32). The results from Mayer-sampling calculations show that the dependence of B_3 on λ is more complex. It is positive at low values of λ because there is only a small number of 'globular' configurations where each of the f_{ij}s in Equation (25) would be positive; most of the 'compact' configurations give less-than-optimum interactions for at least one of the pairs of particles. Increasing λ first just exacerbates this effect, because the LJ energy dominates over the dipolar energy. But at large values of λ, the dipolar interaction must win, and the energetic benefit of the attractive, chain-like structures outweighs the 'entropic' penalty of there being relatively few such structures. Hence, B_3 shows a global maximum, and at high values of λ it becomes negative. The theoretical

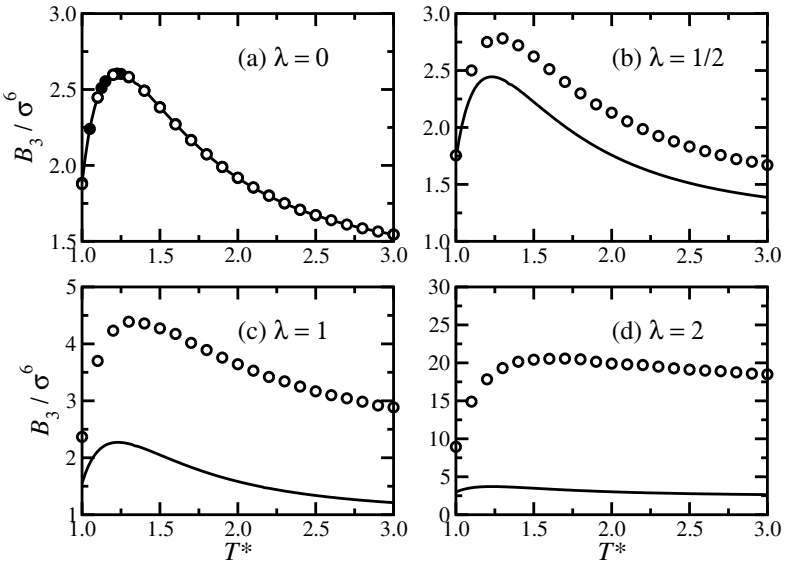

Figure 4. Third virial coefficient B_3 as a function of T^* in zero applied field ($\alpha = 0$): (a) $\lambda = 0$; (b) $\lambda = 1/2$; (c) $\lambda = 1$; (d) $\lambda = 2$. The open symbols are from Mayer sampling, and the lines are from theory. In (a) there are also numerical results taken from Table II of Reference 4 (filled symbols).

expression is rather poor in this case, in that it does not reproduce any kind of global maximum. Moreover, the inset in Figure 5(b) shows that the expansion does not get the initial behaviour correct in the region $0 \leq \lambda \leq 1$. These discrepancies arise from the truncation of Equation (34). In earlier studies of the DHS fluid in zero applied field [45] it was found that an expansion of B_3 up to terms of order λ^{12} was necessary to get reasonable agreement with Mayer-sampling results. This is completely impractical here, as the field-dependence is also required.

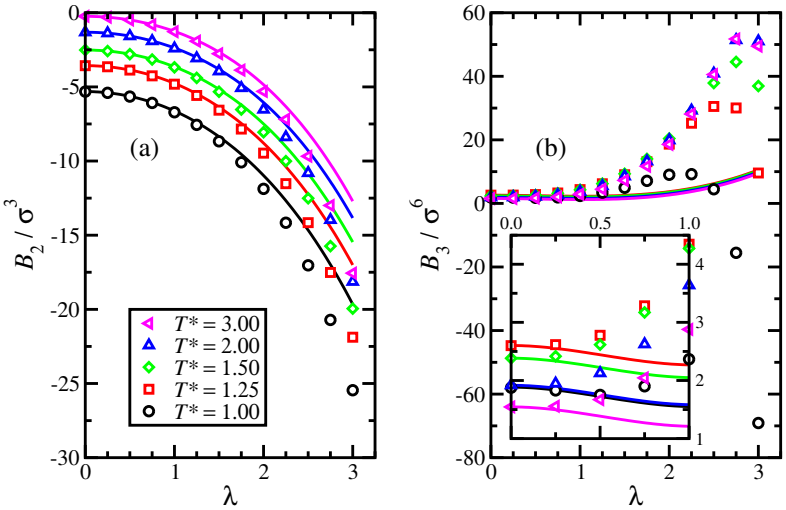

Figure 5. Virial coefficients as functions of λ in zero applied field ($\alpha = 0$): (a) second virial coefficient B_2; (b) third virial coefficient B_3 (with the inset showing data for $0 \leq \lambda \leq 1$). The open symbols are from Mayer sampling, and the lines are from theory.

Finally, the dependences of the virial coefficients on an applied field are considered. The preceding discussion shows that the theory is not reliable at large values of λ, so to avoid clouding the issue, only results with $\lambda = 1$ are considered. Recall that this is a typical value for real ferrofluids, and that in this case, the theoretical expression for B_2 is very accurate, while that for B_3 is inaccurate. Figure 6(a) shows B_2 as a function of α for $\lambda = 1$ and various temperatures T^*. Large values

of α are considered so that the approach to the fully aligned case can be explored; with $\alpha = 1000$, the Langevin magnetisation $L(\alpha) \approx 1 - \alpha^{-1} = 0.999$. The application of a field makes B_2 more negative, due to the increasing statistical weight in Equation (21) of the attractive, chain-like configurations *that are aligned with the field*. The agreement between theory and Mayer sampling is excellent at each of the temperatures considered.

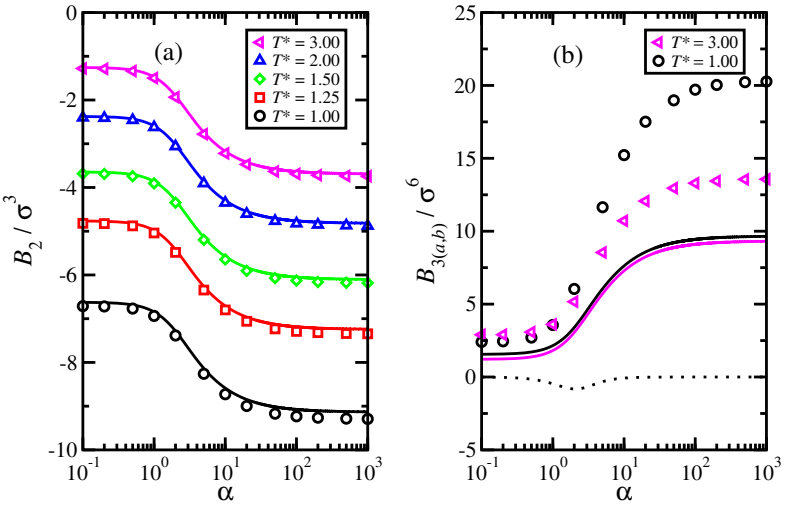

Figure 6. Virial coefficients as functions of α with $\lambda = 1$: (a) second virial coefficient B_2; (b) third virial coefficient B_{3a}. The open symbols are from Mayer sampling, and the solid lines are from theory. In (b), the dotted line is B_{3b} for the case $T^* = 1.00$.

Figure 6(b) shows B_{3a} at two temperatures, $T^* = 1.00$ and 3.00; results for other temperatures fall inbetween, but they are omitted for clarity because the theoretical lines are all similar on that scale. The Mayer-sampling results show that B_{3a} increases with increasing field strength. This is because there are more 'globular' configurations than 'chain-like' configurations; in the former case, aligning the dipoles with the field is likely to increase the energy, while in the latter case, the opposite is true. The theory shows the same basic trends, but the quantitative agreement is poor for precisely the reasons outlined in the zero-field case. To isolate the field-dependence, Figure 7 shows the relative variations of the virial coefficients, defined by

$$R_n(\alpha) = \frac{B_n(\alpha) - B_n(\infty)}{B_n(0) - B_n(\infty)} \tag{38}$$

where of course for the third virial coefficient, B_3 means B_{3a}. As defined, $R_n(0) = 1$ and $R_n(\infty) = 0$. The results from theory and Mayer sampling are in excellent agreement, showing in particular that the origin of the discrepancies in B_{3a} is the truncation in λ, rather than in the field-dependent terms.

Figure 6(b) also shows an example of B_{3b} as a function of α, for the case $T^* = 1.00$ ($\mu^* = 1$). Note that $B_{3b} = 0$ when $\alpha = 0$ and $\alpha = \infty$, as should be clear from Equation (26). The plot just illustrates that B_{3b} is only a minor contribution to B_3, and that B_{3a} accounts for almost all of the variations in B_3.

4.2. *Equation of state*

Figure 8 shows the compressibility factor Z as a function of concentration ρ^* for systems with $\lambda = 1$, at two temperatures, $T^* = 2$ ($\mu^* = \sqrt{2}$) and $T^* = 3$ ($\mu^* = \sqrt{3}$),

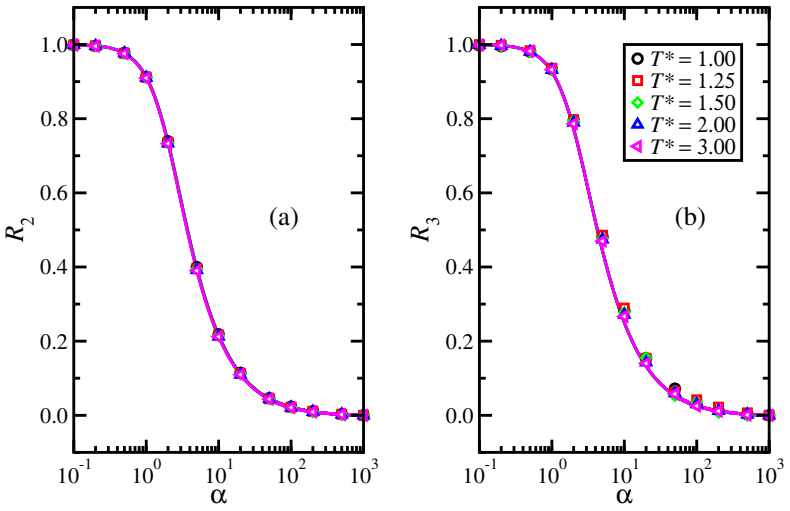

Figure 7. Relative variations of the virial coefficients (38) as functions of α with $\lambda = 1$: (a) relative variation R_2 of the second virial coefficient; (b) relative variation R_3 of the third virial coefficient. The open symbols are from Mayer sampling, and the lines are from theory.

and with field strengths corresponding to $\alpha = 0$, 5, and ∞. Recall that with this value of λ, the theoretical expression for B_2 is practically exact, while that for B_3 is not very reliable (see Figure 6). Nonetheless, $\lambda \sim 1$ in real ferrofluids, and it is therefore important to test the impact of approximating the virial coefficients on the predicted thermodynamic properties. Results were obtained from MD simulations and Equation (17). Figure 8 shows that, even with limited knowledge of B_3, the theory is able to predict basic trends very reliably. Firstly, at each temperature and for a given concentration, the compressibility factor decreases with increasing field strength. Referring to Figure 6, this arises because with increasing α, B_2 becomes more negative (even more 'attractive') and more than compensates for the accompanying increase in B_3. Secondly, for a given field strength and concentration, the compressibility factor increases with increasing temperature. Referring again to Figure 6, B_2 and B_3 increase with increasing temperature as the effects of the attractive interactions are diminished. Finally, Figure 8(b) and (d) shows that the theory gives the correct limiting behaviour at low concentrations, since it is based on a virial expansion, and the theoretical expression for B_2 is very accurate. The theory underestimates the pressure at $\rho^* > 0.05$ due to the underestimation of B_3, as shown in Figure 6.

4.3. *Critical parameters*

Finally, theoretical predictions for the critical parameters are tested against the available simulation data [20, 22]. The critical point (T_c^*, ρ_c^*) is located by solving the simultaneous equations $(\partial P/\partial V)_T = (\partial^2 P/\partial V^2)_T = 0$, with Equation (17) as input. Consider first the reference LJ fluid. Table 1 shows the available, high-precision simulation data from References 60 and 61, and the theory with $Z = Z^{\text{ref}}$. The agreement between the simulated and theoretical critical temperatures is practically perfect, while the theoretical critical density is about 15% lower than the simulation value. In Reference 52, the PVE approach including ΔB_2 and ΔB_3 (with a slightly different choice of effective hard-sphere diameter) gave $T_c^* = 1.28$ and $\rho_c^* = 0.252$.

The available simulation data at different values of $\mu^* > 0$ and H^* are collected in Table 1, and in each case, the LFE prediction is given for comparison. The theory indicates that the critical density decreases with increasing μ^* and H^*, while the

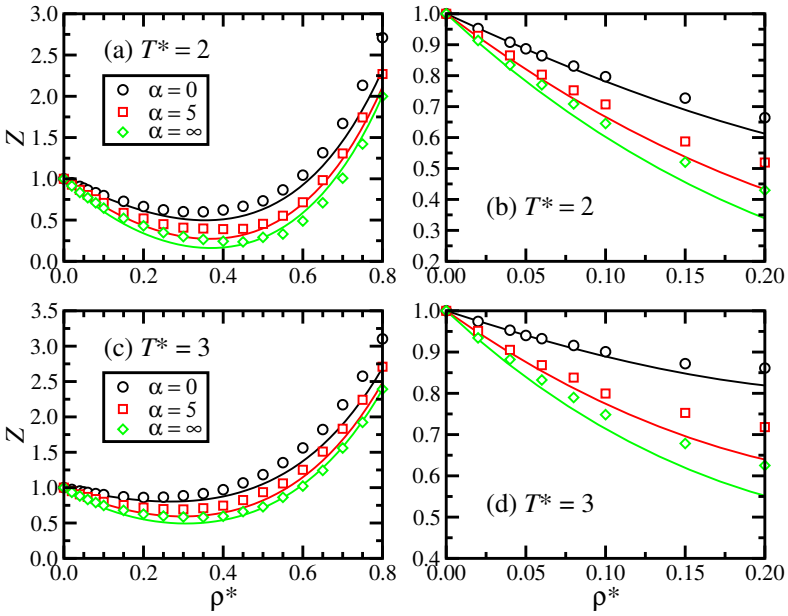

Figure 8. Compressibility factor $Z = \beta P/\rho$ as a function of concentration ρ^* with $\lambda = 1$: (a) and (b) $T^* = 2$ ($\mu^* = \sqrt{2}$); (c) and (d) $T^* = 3$ ($\mu^* = \sqrt{3}$). The points are from MD simulations, and the lines are from the LFE theory, Equation (17).

simulation data suggest that it is almost independent of the conditions. It is difficult to draw any strong conclusions here, because the critical density is notoriously difficult to pin down precisely using molecular simulations. The variations of the critical temperature with changing μ^* and H^* are more robust, and to make a more visual comparison, Figure 9 shows a plot of T_c^* from simulation against that from theory. The theory is very accurate with $\mu^* = 0$ and $\mu^* = 1$, but deviations become apparent with larger values of μ^*. Of course, this arises primarily from the generally poor description of B_3 for $\mu^* \geq \sqrt{2}$, as shown in Figure 2.

The accuracy of the LFE theory in predicting the critical parameters with low values of μ^*, and the equations of state at moderately supercritical temperatures, show that it is basically correct. The expressions for the virial coefficients are reasonably good over broad ranges of temperature, provided that the dipole moment is not too high. These observations suggest that the LFE theory presented here should be successful in predicting the vapour-liquid coexistence properties just below T_c. At much lower temperatures, though, the expressions for B_2 and B_3 in terms of λ will become unreliable, and then significant errors are likely to result. That is not to say that the LFE theory itself should become less accurate at low temperatures, and indeed it would be interesting to test the theory systematically in terms of the phase diagrams predicted for some model systems.

5. Conclusions

In this work, the virial coefficients and thermodynamics of the Stockmayer fluid in an applied field have been determined from theory and by computation. The two essential ingredients of the theory are explicit expressions for the first few virial coefficients, and the logarithmic free energy approach which captures some of the effects of higher virial coefficients in the sense of an approximate resummation.

Analytical expressions for the virial coefficients have been tested critically against the results from Mayer-sampling calculations. The comparison shows that the expression for the second virial coefficient is highly accurate over realistic ranges of

Table 1. Critical parameters for the Stockmayer fluid in an applied field from simulation [20, 22, 60, 61] and the LFE theory.

μ^*	H^*	T_c^*	ρ_c^*	Reference	T_c^* (theory)	ρ_c^* (theory)
0	0.0	1.3120(7)	0.316(1)	[60]	1.3118	0.2679
0	0.0	1.3145(2)	0.316(1)	[61]	1.3118	0.2679
1	0.0	1.41(1)	0.30(1)	[20]	1.4730	0.2747
1	1.0	1.44(1)	0.32(1)	[20]	1.4887	0.2746
1	2.0	1.49(1)	0.33(1)	[20]	1.5196	0.2735
1	3.0	1.51(1)	0.32(1)	[20]	1.5469	0.2712
1	0.0	1.4091(41)	0.3122(9)	[22]	1.4730	0.2747
1	1.0	1.4273(87)	0.3127(18)	[22]	1.4887	0.2746
1	1.5	1.4428(84)	0.3151(19)	[22]	1.5039	0.2742
1	2.0	1.462(11)	0.3113(25)	[22]	1.5196	0.2735
$\sqrt{2}$	0.0	1.6044(54)	0.3115(14)	[22]	1.7881	0.2730
$\sqrt{2}$	0.4	1.6097(59)	0.3091(17)	[22]	1.7945	0.2728
$\sqrt{2}$	0.8	1.6436(64)	0.3084(18)	[22]	1.8112	0.2723
$\sqrt{2}$	1.2	1.6786(81)	0.3082(17)	[22]	1.8332	0.2713
2.5	0.0	2.63(1)	0.29(1)	[20]	3.2892	0.2267
2.5	0.5	2.71(1)	0.285(1)	[20]	3.3075	0.2262
2.5	1.0	2.78(1)	0.285(1)	[20]	3.3541	0.2249
2.5	2.0	2.89(1)	0.302(1)	[20]	3.4694	0.2208
2.5	5.0	3.15(1)	0.278(1)	[20]	3.6760	0.2098
2.5	∞	3.64(1)	0.303(1)	[20]	4.0400	0.1952

temperature and dipole moment, and over the entire range of applied field strengths (from zero to infinity). An accurate expression for the third virial coefficient is more challenging to obtain, being hampered by truncation of the expansion in terms of the dipolar coupling constant. Nonetheless, the relative changes in both the second and third virial coefficient over the full range of field strengths have been obtained essentially exactly. It is therefore clear that to improve the expressions further, one need concentrate on the expansion with respect to the dipolar coupling constant.

There seems little prospect of determining accurate analytical expressions for the higher virial coefficients in the presence of a field, but the logarithmic free energy theory mitigates the usual problems arising from truncating the virial expansion – or at least, correcting only the first two virial coefficients of a reference system to include additional interactions. This has been demonstrated by computing the equation of state and critical parameters, and comparing them against new and existing simulation data. The results are encouraging, with the theory capturing faithfully the dependences of the thermodynamic properties on dipole moment and applied field strength, despite knowledge of the third virial coefficient being somewhat limited. In general, the accuracy of the LFE approach should depend on the magnitudes and signs of the cumulant coefficients I_n, and hence on the precise numerical values of the virial coefficients B_n. This work, in combination with earlier studies [44, 45], shows that it works very well for dipolar interactions of realistic strengths (coupling constant $\lambda \sim 1$) and all values of the applied field strength.

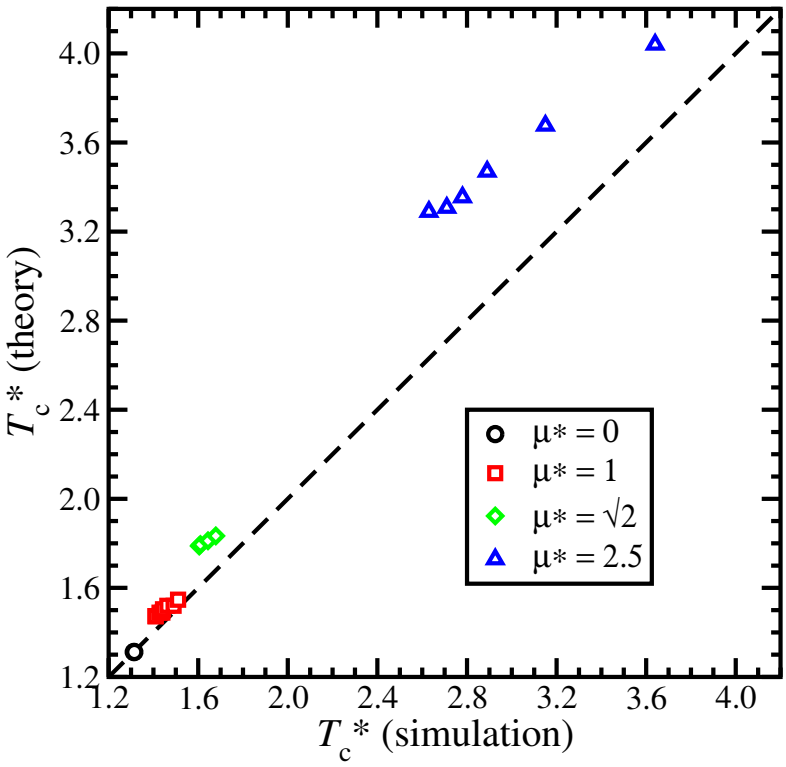

Figure 9. The critical temperatures from simulation [20, 22, 60, 61] and LFE theory plotted against each other. Data are separated in to groups with $\mu^* = 0$ (black circles), $\mu^* = 1$ (red squares), $\mu^* = \sqrt{2}$ (green diamonds), and $\mu^* = 2.5$ (blue triangles). In each group, the critical temperature increases with increasing field strength H^*, as given in Table 1.

Funding

E.A.E. and A.O.I. gratefully acknowledge research funding from the Ministry of Education and Science of the Russian Federation (Agreement No. 3.12.2014/K, Contract No. 02.A03.21.0006). J.O.S. was supported by the Engineering and Physical Sciences Research Council (UK) through the provision of a studentship. E.A.E. and P.J.C. thank the Ural Federal University for supporting collaborative visits between the Edinburgh and Ekaterinburg groups.

References

[1] W.H. Stockmayer, J. Chem. Phys. **9**, 398 (1941).
[2] J.S. Rowlinson, J. Chem. Phys. **19**, 827 (1951).
[3] J.S. Rowlinson, J. Chem. Phys. **19**, 831 (1951).
[4] J.A. Barker, P.J. Leonard and A. Pompe, J. Chem. Phys. **44**, 4206 (1966).
[5] P.I.C. Teixeira, J.M. Tavares and M.M. Telo da Gama, J. Phys.: Condens. Matter **12**, R411 (2000).
[6] R.E. Rosensweig, *Ferrohydrodynamics* (Dover Publications, Inc., New York, 1998).
[7] A.O. Ivanov, S.S. Kantorovich, E.N. Reznikov, C. Holm, A.F. Pshenichnikov, A.V. Lebedev, A. Chremos and P.J. Camp, Phys. Rev. E **75**, 061405 (2007).
[8] A.O. Ivanov, S.S. Kantorovich, E.N. Reznikov, C. Holm, A.F. Pshenichnikov, A.V. Lebedev, A. Chremos and P.J. Camp, Magnetohydrodynamics **43**, 393 (2007).
[9] P.J. Camp, E.A. Elfimova and A.O. Ivanov, J. Phys.: Condens. Matter **26**, 456002 (2014).
[10] A.O. Ivanov and E.A. Elfimova, J. Mag. Mag. Mater. **374**, 327 (2015).
[11] M.E. van Leeuwen and B. Smit, Phys. Rev. Lett. **71**, 3991 (1993).
[12] M.E. van Leeuwen, B. Smit and E.M. Hendriks, Mol. Phys. **78**, 271 (1993).
[13] M.E. van Leeuwen, Mol. Phys. **82**, 383 (1994).

[14] K.C. Ng, J.P. Valleau, G.M. Torrie and G.N. Patey, Mol. Phys. **38**, 781 (1979).
[15] J.M. Caillol, J. Chem. Phys. **98**, 9835 (1993).
[16] J.J. Weis and D. Levesque, Phys. Rev. Lett. **71**, 2729 (1993).
[17] D. Levesque and J.J. Weis, Phys. Rev. E **49**, 5131 (1994).
[18] M.J. Stevens and G.S. Grest, Phys. Rev. Lett. **72**, 3686 (1994).
[19] M.J. Stevens and G.S. Grest, Phys. Rev. E **51**, 5962 (1995).
[20] M.J. Stevens and G.S. Grest, Phys. Rev. E **51**, 5976 (1995).
[21] S.C. McGrother, D.C. Williamson and G. Jackson, J. Chem. Phys. **104**, 6755 (1996).
[22] D. Boda, J. Winkelmann, J. Liszi and I. Szalai, Mol. Phys. **87**, 601 (1996).
[23] I. Szalai, D. Henderson, D. Boda and K.Y. Chan, J. Chem. Phys. **110**, 7348 (1999).
[24] P.J. Camp, J.C. Shelley and G.N. Patey, Phys. Rev. Lett. **84**, 115 (2000).
[25] T. Kristóf, J. Liszi and I. Szalai, Phys. Rev. E **69**, 062106 (2004).
[26] R. Hentschke, J. Bartke and F. Pesth, Phys. Rev. E **75**, 011506 (2007).
[27] J. Bartke and R. Hentschke, Phys. Rev. E **75**, 061503 (2007).
[28] G. Ganzenmüller and P.J. Camp, J. Chem. Phys. **126**, 191104 (2007).
[29] G. Ganzenmüller and P.J. Camp, J. Chem. Phys. **127**, 154504 (2007).
[30] A.O. Ivanov, S.S. Kantorovich and P.J. Camp, Phys. Rev. E **77**, 013501 (2008).
[31] R. Hentschke and J. Bartke, Phys. Rev. E **77**, 013502 (2008).
[32] N.G. Almarza, E. Lomba, C. Martín and A. Gallardo, J. Chem. Phys. **129**, 234504 (2008).
[33] R. Jia and R. Hentschke, Phys. Rev. E **80**, 051502 (2009).
[34] G. Ganzenmüller, G.N. Patey and P.J. Camp, Mol. Phys. **107**, 403 (2009).
[35] L. Rovigatti, J. Russo and F. Sciortino, Phys. Rev. Lett. **107**, 237801 (2011).
[36] L. Rovigatti, J. Russo and F. Sciortino, Soft Matter **8**, 6310 (2012).
[37] S. Dussi, L. Rovigatti and F. Sciortino, Mol. Phys. **111**, 3608 (2013).
[38] B. Groh and S. Dietrich, Phys. Rev. E **53**, 2509 (1996).
[39] S. Klapp and F. Forstmann, Phys. Rev. E **60**, 3183 (1999).
[40] J.B. Hayter and R. Pynn, Phys. Rev. Lett. **49**, 1103 (1982).
[41] S.H.L. Klapp and G.N. Patey, J. Chem. Phys. **112**, 3832 (2000).
[42] A.O. Ivanov and E.V. Novak, Colloid J. **69**, 302 (2007).
[43] E.A. Elfimova and A.O. Ivanov, J. Exp. Theor. Phys. **111**, 146 (2010).
[44] E.A. Elfimova, A.O. Ivanov and P.J. Camp, Phys. Rev. E **88**, 042310 (2013).
[45] E.A. Elfimova, A.O. Ivanov and P.J. Camp, Phys. Rev. E **86**, 021126 (2012).
[46] S. Caracciolo, B.M. Mognetti and A. Pelissetto, J. Chem. Phys. **125**, 094903 (2006).
[47] S. Caracciolo, B.M. Mognetti and A. Pelissetto, Macromol. Theory Simul. **17**, 67 (2008).
[48] J.K. Singh and D.A. Kofke, Phys. Rev. Lett. **92**, 220601 (2004).
[49] K. Aim and I. Nezbeda, Fluid Phase Equil. **12**, 235 (1983).
[50] I. Nezbeda, Fluid Phase Equil. **87**, 237 (1993).
[51] J. Kolafa and I. Nezbeda, Fluid Phase Equil. **100**, 1 (1994).
[52] I. Nezbeda and W.R. Smith, Fluid Phase Equil. **216**, 183 (2004).
[53] J. Krejčí and I. Nezbeda, Fluid Phase Equil. **314**, 156 (2012).
[54] J.A. Barker and D. Henderson, J. Chem. Phys. **47**, 4714 (1967).
[55] J.P. Hansen and I.R. McDonald, *Theory of Simple Liquids*, 3rd ed. (Academic Press, London, 2006).
[56] N.F. Carnahan and K.E. Starling, J. Chem. Phys. **51**, 635 (1969).
[57] LAMMPS Molecular Dynamics Simulator http://lammps.sandia.gov.
[58] S. Plimpton, J. Comp. Phys. **117**, 1 (1995).
[59] S. Banerjee, R.B. Griffiths and M. Widom, J. Stat. Phys. **93**, 109 (1998).
[60] J.J. Potoff and A.Z. Panagiotopoulos, J. Chem. Phys. **109**, 10914 (1998).
[61] W. Shi and J.K. Johnson, Fluid Phase Equil. **187-188**, 171 (2001).

Appendix A. Integrals appearing in B_2

Inserting Equation (30) in to Equation (21) with terms up to $k + l = 4$ gives the following terms.

A.1. $k = 0,\ l = 1, 2, 3$

$$\frac{1}{l!}\int \mathrm{d}\boldsymbol{r}_{12}(f_{12}^{\mathrm{HS}}+1)\langle(-\beta u_{12}^{\mathrm{d}})^{l}\rangle \tag{A1}$$

These integrals are evaluated in the Supplemental Material of Reference 44.

A.2. $k = 0,\ l = 4$

$$\begin{aligned}&\frac{1}{24}\int \mathrm{d}\boldsymbol{r}_{12}(f_{12}^{\mathrm{HS}}+1)\langle(-\beta u_{12}^{\mathrm{d}})^{4}\rangle\\&=\frac{\pi\lambda^{4}\sigma^{12}}{315d^{9}}\left[\frac{116L^{2}(\alpha)}{\alpha^{2}}-\frac{44L(\alpha)}{\alpha}-\left(\frac{395}{\alpha^{3}}-\frac{28}{\alpha}\right)L_{3}(\alpha)L(\alpha)-\left(\frac{105}{\alpha^{2}}-\frac{140}{\alpha^{4}}\right)L_{3}^{2}(\alpha)\right.\\&\left.+\frac{113L_{3}(\alpha)}{\alpha^{2}}+8\right]\end{aligned} \tag{A2}$$

A.3. $k = 1, 2, 3,\ l = 1$

$$\frac{1}{k!}\int \mathrm{d}\boldsymbol{r}_{12}(f_{12}^{\mathrm{HS}}+1)(-\beta u_{12}^{\mathrm{a}})^{k}\langle-\beta u_{12}^{\mathrm{d}}\rangle = 0 \tag{A3}$$

A.4. $k = 1,\ l = 2$

$$\frac{1}{2}\int \mathrm{d}\boldsymbol{r}_{12}(f_{12}^{\mathrm{HS}}+1)(-\beta u_{12}^{\mathrm{a}})\langle(-\beta u_{12}^{\mathrm{d}})^{2}\rangle = \frac{32\pi\lambda^{2}\sigma^{3}}{675T^{*}}\left[5+L_{3}^{2}(\alpha)\right] \tag{A4}$$

A.5. $k = 2,\ l = 2$

$$\frac{1}{4}\int \mathrm{d}\boldsymbol{r}_{12}(f_{12}^{\mathrm{HS}}+1)(-\beta u_{12}^{\mathrm{a}})^{2}\langle(-\beta u_{12}^{\mathrm{d}})^{2}\rangle = \frac{256\pi\lambda^{2}\sigma^{3}}{14175(T^{*})^{2}}\left[5+L_{3}^{2}(\alpha)\right] \tag{A5}$$

A.6. $k = 1,\ l = 3$

$$\begin{aligned}&\frac{1}{6}\int \mathrm{d}\boldsymbol{r}_{12}(f_{12}^{\mathrm{HS}}+1)(-\beta u_{12}^{\mathrm{a}})\langle(-\beta u_{12}^{\mathrm{d}})^{3}\rangle\\&=\frac{8\pi\lambda^{3}\sigma^{3}}{945T^{*}}\left[\frac{2L(\alpha)L_{3}(\alpha)}{\alpha}-\frac{5L_{3}^{2}(\alpha)}{\alpha^{2}}+4L^{2}(\alpha)\right]\end{aligned} \tag{A6}$$

Appendix B. Integrals appearing in B_{3a} and B_{3b}

Inserting Equation (30) in to Equations (25) and (26), and retaining only those terms up to λ^3 and $1/T^*$, leads to considerable simplifications. Firstly, the expres-

sion for B_{3a} becomes

$$
\begin{aligned}
&B_{3a} = B_3^{\mathrm{LJ}} \\
&-\frac{1}{3}\int \mathrm{d}\boldsymbol{r}_{12}\int \mathrm{d}\boldsymbol{r}_{13}\Big\{3(f_{12}^{\mathrm{HS}}+1)f_{13}^{\mathrm{HS}}f_{23}^{\mathrm{HS}}\Big[\langle -\beta u_{12}^{\mathrm{d}}\rangle + \frac{1}{2}\langle(-\beta u_{12}^{\mathrm{d}})^2\rangle + \frac{1}{6}\langle(-\beta u_{12}^{\mathrm{d}})^3\rangle \\
&+(-\beta u_{12}^{\mathrm{a}})\langle -\beta u_{12}^{\mathrm{d}}\rangle\Big] \\
&+3(f_{12}^{\mathrm{HS}}+1)(f_{13}^{\mathrm{HS}}+1)f_{23}^{\mathrm{HS}}\Big[2(-\beta u_{13}^{\mathrm{a}})\langle -\beta u_{12}^{\mathrm{d}}\rangle + \langle(-\beta u_{12}^{\mathrm{d}})(-\beta u_{13}^{\mathrm{d}})\rangle \\
&+\langle(-\beta u_{12}^{\mathrm{d}})^2(-\beta u_{13}^{\mathrm{d}})\rangle\Big] \\
&+(f_{12}^{\mathrm{HS}}+1)(f_{13}^{\mathrm{HS}}+1)(f_{23}^{\mathrm{HS}}+1)\langle(-\beta u_{12}^{\mathrm{d}})(-\beta u_{13}^{\mathrm{d}})(-\beta u_{23}^{\mathrm{d}})\rangle\Big\}. \qquad \text{(B1)}
\end{aligned}
$$

These types of integrals were considered in Reference 44. The terms proportional to $(-\beta u_{12}^{\mathrm{a}})\langle -\beta u_{12}^{\mathrm{d}}\rangle$ and $(-\beta u_{13}^{\mathrm{a}})\langle -\beta u_{12}^{\mathrm{d}}\rangle$ disappear after the orientational and positional integrations. The remaining integrals do not depend on u_{ij}^{a}, and are given in the Supplemental Material of Reference 44. At the same level of approximation, the expression for B_{3b} reads

$$
\begin{aligned}
&B_{3b} \\
&= \int \mathrm{d}\boldsymbol{r}_{12}\int \mathrm{d}\boldsymbol{r}_{13}(f_{12}^{\mathrm{HS}}+1)(f_{13}^{\mathrm{HS}}+1)\left[\langle -\beta u_{12}^{\mathrm{d}}\rangle\langle -\beta u_{13}^{\mathrm{d}}\rangle - \langle(-\beta u_{12}^{\mathrm{d}})(-\beta u_{13}^{\mathrm{d}})\rangle\right] \\
&+\int \mathrm{d}\boldsymbol{r}_{12}\int \mathrm{d}\boldsymbol{r}_{13}(f_{12}^{\mathrm{HS}}+1)(f_{13}^{\mathrm{HS}}+1)\left[\langle(-\beta u_{12}^{\mathrm{d}})^2\rangle\langle -\beta u_{13}^{\mathrm{d}}\rangle - \langle(-\beta u_{12}^{\mathrm{d}})^2(-\beta u_{13}^{\mathrm{d}})\rangle\right] \qquad \text{(B2)}
\end{aligned}
$$

and there are no terms that depend on u_{ij}^{a}. Hence, the integrals are identical to those presented in the Supplemental Material of Reference 44.